energies

MDPI

Article

Impact Study of PMSG-Based Wind Power Penetration on Power System Transient Stability Using EEAC Theory

Zhongyi Liu [1,2,*], Chongru Liu [1], Gengyin Li [1], Yong Liu [2] and Yilu Liu [2]

Received: 17 September 2015; Accepted: 16 November 2015; Published: 26 November 2015
Academic Editor: Frede Blaabjerg

[1] State Key Laboratory of Alternate Electrical Power System with Renewable Energy Sources, North China Electric Power University, Beijing 102206, China; chongru.liu@ncepu.edu.cn (C.L.); ligy@ncepu.edu.cn (G.L.)
[2] Department of Electrical Engineering & Computer Science, University of Tennessee, Knoxville, TN 37996, USA; yliu66@utk.edu (Y.L.); liu@utk.edu (Y.L.L.)
* Correspondence: liuzhongyi1988@sina.com; Tel.: +86-18810426707

Abstract: Wind turbines with direct-driven permanent magnet synchronous generators (PMSGs) are widely used in wind power generation. According to the dynamic characteristics of PMSGs, an impact analysis of PMSG-based wind power penetration on the transient stability of multi-machine power systems is carried out in this paper based on the theory of extended equal area criterion (EEAC). Considering the most severe PMSG integration situation, the changes in the system's equivalent power-angle relationships after integrating PMSGs are studied in detail. The system's equivalent mechanical input power and the fault period electrical output power curves are found to be mainly affected. The analysis demonstrates that the integration of PMSGs can cause either detrimental or beneficial effects on the system transient stability. It is determined by several factors, including the selection of the synchronous generators used to balance wind power, the reactive power control mode of PMSGs and the wind power penetration level. Two different simulation systems are also adopted to verify the analysis results.

Keywords: permanent magnet synchronous generators (PMSGs); transient stability; extended equal area criterion (EEAC); multi-machine power system

1. Introduction

Wind energy has developed quickly in recent years. The total capacity of the globally installed wind turbine generators at the end of 2014 was 369.6 GW, representing a cumulative market growth of more than 16% compared with 2013 [1]. Current wind energy conversion technologies mainly use wind turbines with direct-driven permanent magnet synchronous generators (PMSGs) or wind turbines with doubly-fed induction generators (DFIGs) [2]. Compared with DFIGs, PMSGs have the following advantages: a PMSG allows the generator to operate at low speed without a gearbox. This reduces the weight and dimensions of nacelle equipment, mechanical losses in operation as well as maintenance requirements. A PMSG can also contribute to the grid voltage support by generating more reactive power since it is interfaced with the power system via a full-scale back to back converter. These properties have made PMSGs become popular, even though converter losses increase [3,4].

After integrating PMSGs, a power system can experience significant changes in its dynamic characteristics [5]. The impact of PMSG-based wind power penetration on an existing power system, especially the system transient stability, must be examined carefully [6]. There is some

literature studying this problem. For instance, in [7], the transient stability margins of a one-machine infinite-bus system (OMIB system) and a four-machine system were both enlarged by integrating PMSGs. In [8], a Monte Carlo simulation was carried out on a ten-machine system. The results presented that the system transient stability became better in most situations because PMSGs were integrated. The study in [9] showed the manner in which PMSGs inject reactive power into the system can be critical in maintaining the rotor angle stability of a 39-bus system. References [10–12] also studied the reactive power control of PMSGs during steady and transient states. The transient stability of their simulation cases were improved by injecting more reactive power from PMSGs. The above literature unveiled the fact that there are close correlations between the integration of PMSGs and power system transient stability. However, their conclusions were obtained only from the simulation results of their respective test systems. These conclusions are always limited to the particular systems they used and may be not applicable in other different systems. In addition, the mechanisms behind their simulation phenomena have not been studied enough or explained sufficiently. Therefore, a deeper mechanism analysis without depending on any particular system needs to be carried out to find out some influence rules of integrating PMSGs on the power system transient stability.

The work in [13,14] tried to give a theoretical explanation for the mechanism of how integrating PMSGs influences the transient stability of OMIB systems. In their research, the equivalent impedance seen by a conventional synchronous generator was examined in the presence of PMSGs. They found that the system transient stability can be either degraded or improved due to the different manners of PMSGs' power output. However, their analysis method is not suitable for the study of multi-machine systems, so the impact of integrating PMSGs on the transient stability of multi-machine power systems still cannot be explained clearly. Further studies are thus needed to analyze more complex networks.

For the transient stability assessment of multi-machine power systems, extended equal area criterion (EEAC) is a widely used method [15–17]. According to the theory of EEAC, the transient stability problem of a large power system can be reduced to a sole algebraic equation that is derived from the well-known equal area criterion [18], so the transient stability mechanism of large power systems can be more easily analyzed and explained based on the EEAC theory. In [19], EEAC theory had already been adopted to analyze the mechanism of DFIGs' effects on the power system transient stability, but EEAC theory has never been used in studies of power systems with PMSGs. The application of EEAC theory in the impact analysis of PMSGs should be explored.

In this paper, we focus on the impact of PMSG-based wind power penetration on the transient stability of multi-machine power systems. After integrating PMSGs, the mechanisms and rules of the changes in the system transient stability are analyzed based on the EEAC theory. Several scenarios of system operation with PMSGs are studied, considering the most severe situation of PMSG integration, different synchronous generators used to balance wind power, and different reactive power control modes of PMSGs. The rest of this paper is organized as follows: Section 2 introduces a simplified model of PMSGs for transient stability studies and discusses the transient behaviors of PMSGs under different control modes; Section 3 presents the basic theory of EEAC; Section 4 makes the influence analysis of integrating PMSGs on the system transient stability in detail by using EEAC theory; Section 5 verifies the influence rules of PMSGs, which are obtained in Section 4, by the dynamic simulations in Western Systems Coordinating Council (WSCC) 3-machine-9-bus system and Institute of Electrical and Electronics Engineers (IEEE) 10-mahicne-39-bus system; and Section 6 summarizes conclusions.

2. PMSG Modeling and Transient Behavior Analysis

2.1. PMSG Simplified Model for Transient Stability Study

PMSG is a variable speed wind turbine generator with a full-scale power electronic interface. Its configuration is shown in Figure 1. The wind turbine and the generator of a PMSG are decoupled from the network by the full-scale power converters. Based on the chopper action, a PMSG also has low voltage ride through capability. The grid side disturbances thus have little impact on the mechanical parts of a PMSG [20]. Moreover, in transient stability studies, the variation of wind speed is always neglected due to the short time scale [21], so the PMSG rotation speed remains constant during the transient period. The wind turbine and the generator of a PMSG do not show any dynamic behavior. Only the dynamics of the grid side converter can be seen by the grid [13]. Therefore, except the grid side converter and its controller, all other controllers and elements of a PMSG can be neglected for simplification.

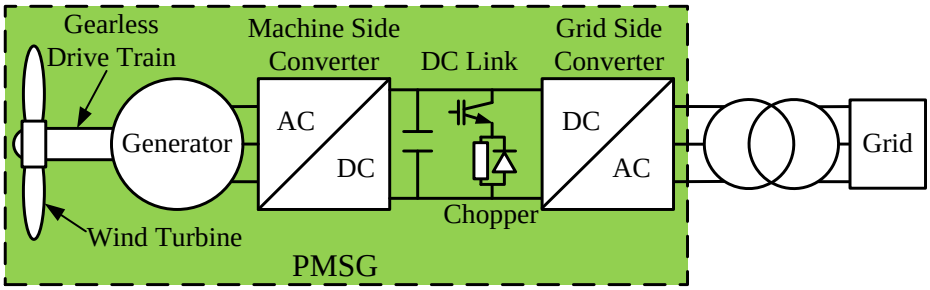

Figure 1. Configuration of a wind turbine with direct-driven permanent magnet synchronous generator (PMSG).

In addition, the grid side converter has rapid current control loop, which is able to achieve a current rise time of only 3 ms [22], so the control process of the current control loop can be ignored too for further simplification. The grid side converter thus no longer needs to be modeled. Only the outer power control loop of the grid side converter controller is reserved to give the value of the current outputted by a PMSG. As a result, in transient stability studies, a PMSG can be modeled as a controlled current source as shown in Figure 2 [10]. I_{gd}, I_{gq} are the active and reactive components of the grid side current, respectively.

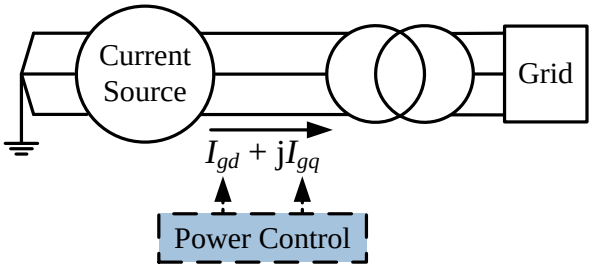

Figure 2. Controlled current source model of a PMSG.

The detailed control process of the PMSG controlled current source model is shown in Figure 3 [23]. P_g, P_{gref} are the actual and reference values of the active power output of a PMSG respectively. Q_g, Q_{gref} are the actual and reference values of the reactive power output of a PMSG respectively. I_{gdcmd}, I_{gqcmd} are the reference values of I_{gd} and I_{gq} respectively. Before obtaining I_{gd} and I_{gq}, the amplitudes of I_{gdcmd} and I_{gqcmd} need to be limited according to the converter's maximum current rating, which is denoted by I_{max}. The validity of using the PMSG controlled current source

model in transient stability studies has been proved in [23] through the comparison with the practical measurement data.

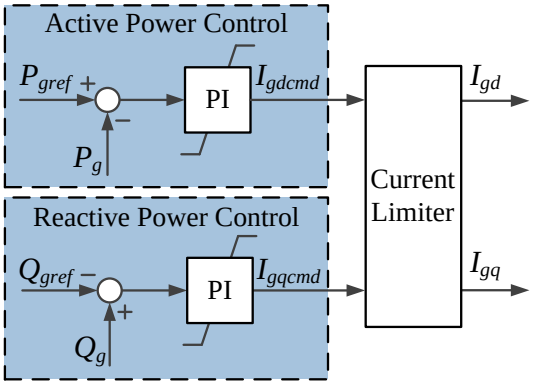

Figure 3. Control process of the PMSG controlled current source model.

2.2. PMSG Transient Behavior Analysis

Since a PMSG can be modeled as a controlled current source in transient stability studies, its grid side performance is mainly determined by the output current. With different power control modes, the output current of a PMSG will show different dynamic behaviors. Traditionally, a PMSG is controlled to operate with the unity power factor [10]. In this mode, a PMSG has no reactive power exchange with the network, but recent grid codes require PMSGs to generate more reactive power during the abnormal low voltage periods [11]. For example, as stated by the SDLWindV grid code, the reactive component of the output current of a PMSG is required to increase by 2% for each 1% reduction in the unit terminal voltage when this voltage deviation is beyond the dead band [24].

In transient stability studies, short circuit faults in networks are always concerned. Before faults happen, systems operate steadily. The output current of a PMSG with the unity power factor control mode holds a constant value, I_{gdO} + j0. I_{gdO} is the pre-fault value of I_{gd}. A PMSG with the reactive power support control mode has the same output current since the voltage deviation of the PMSG's grid side terminal is within the dead band during the pre-fault period.

During the fault period, the grid voltage drops. A PMSG outputs less active power than in pre-fault operation due to the low voltage limitation. A PMSG with the unity power factor control mode still outputs zero reactive current while its active output current increases to I_{max}, in order to promote the active power output. The output current of a PMSG with the unity power factor control mode thus becomes I_{max} + j0. Comparatively, a PMSG with the reactive power support control mode outputs more reactive current. Its output current becomes I_{gdD} + jI_{gqD}. I_{gdD}, I_{gqD} are the during fault values of I_{gd} and I_{gq} respectively. I_{gqD} is controlled to comply with grid codes. Under the reactive power support control mode, the converter capacity is preferentially used to carry out the reactive power control [25]. I_{gdD} is limited by I_{max} as follows:

$$I_{gdD} = \sqrt{I_{max}^2 - I_{gqD}^2} \tag{1}$$

During the post-fault period, grid voltage recovers. The output power of a PMSG is able to track the maximum wind power again and thus stays constant without oscillations [20]. Considering the fast control capability of converters, the output current of a PMSG can be rapidly regulated back to its pre-fault value, which is I_{gdO} + j0, no matter what kind of power control mode is adopted [26].

3. EEAC Theory

EEAC is widely used in the transient stability studies of multi-machine power systems. The basic theory of EEAC is summarized as follows: in a multi-machine power system, the motion of the i-th synchronous generator is described by:

$$\begin{cases} \dfrac{\mathrm{d}\delta_i}{\mathrm{d}t} = \omega_i - 1 \\ M_i \dfrac{\mathrm{d}\omega_i}{\mathrm{d}t} = P_{mi} - P_{ei} \end{cases} \qquad (i = 1, 2, \cdots, n) \tag{2}$$

where, δ_i, ω_i, M_i, P_{mi}, P_{ei} are the rotor angle, rotor speed, inertia coefficient, mechanical input power and the electrical output power of the i-th synchronous generator respectively.

When the system experiences a disturbance, such as a short circuit fault, all the synchronous generators in the system can be divided into two groups. One is the specific cluster, which is denoted by S. It consists of the critical synchronous generators that are the machines affected by the disturbance the most severely. The other one is the remaining cluster, which is denoted by A. It consists of all the remaining synchronous generators except for the critical ones. In the transient period, the critical machines move apart from the remaining ones. Considering the relative motion of the critical synchronous generators with respect to the remaining synchronous generators, a multi-machine power system can be equivalent to an OMIB system [18]. The motion of the equivalent OMIB system is described by:

$$M \frac{\mathrm{d}^2\delta}{\mathrm{d}t^2} = P_m - P_e \tag{3}$$

where, M, δ, P_m, P_e are the equivalent inertia coefficient, equivalent rotor angle, equivalent mechanical input power and the equivalent electrical output power of the whole system respectively. Their specific expressions are described by:

$$\begin{cases} M = \dfrac{M_S M_A}{M_S + M_A} & M_S = \sum\limits_{i \in S} M_i & M_A = \sum\limits_{j \in A} M_j \\ \delta = \delta_S - \delta_A & \delta_S = \dfrac{\sum\limits_{i \in S} M_i \delta_i}{M_S} & \delta_A = \dfrac{\sum\limits_{j \in A} M_j \delta_j}{M_A} \end{cases} \tag{4}$$

$$P_m = \frac{1}{M_S + M_A} \left(M_A \sum_{i \in S} P_{mi} - M_S \sum_{j \in A} P_{mj} \right) \tag{5}$$

$$P_e = \frac{1}{M_S + M_A} \left(M_A \sum_{i \in S} P_{ei} - M_S \sum_{j \in A} P_{ej} \right) = P_C + P_{max} \sin(\delta - \gamma) \tag{6}$$

where, M_S, δ_S are the equivalent inertia coefficient and the equivalent rotor angle of the specific cluster respectively. M_A, δ_A are the equivalent inertia coefficient and the equivalent rotor angle of the remaining cluster respectively. M_j, δ_j, P_{mj}, P_{ej} are the inertia coefficient, rotor angle, mechanical input power and the electrical output power of the j-th synchronous generator respectively. P_C, P_{max}, γ are the coefficients of the sinusoidal expression of P_e, which are described by:

$$\begin{cases} P_C = \dfrac{M_A}{M_S + M_A} \sum\limits_{i \in S} \sum\limits_{k \in S} E_i E_k G_{ik} - \dfrac{M_S}{M_S + M_A} \sum\limits_{j \in A} \sum\limits_{l \in A} E_j E_l G_{jl} \\ P_{max} = \sqrt{C^2 + D^2} \qquad \gamma = -\tan^{-1} \dfrac{C}{D} \\ C = \dfrac{M_A - M_S}{M_S + M_A} \sum\limits_{i \in S} \sum\limits_{j \in A} E_i E_j G_{ij} \qquad D = \sum\limits_{j \in A} \sum\limits_{i \in S} E_i E_j B_{ij} \end{cases} \tag{7}$$

where, E_i, E_j, E_k, E_l are the internal voltages of the i-th, j-th, k-th and l-th synchronous generators respectively. G_{ij}, G_{ik}, G_{jl} are the conductances between the internal generator nodes of the i-th and j-th synchronous generators, the i-th and k-th synchronous generators, the j-th and l-th synchronous generators respectively. B_{ij} is the susceptance between the internal generator nodes of the i-th and j-th synchronous generators. C and D are the intermediate variables. $G_{ij} + \mathrm{j}B_{ij}$ is an element of the admittance matrix reduced at the internal generator nodes.

Traditionally, M_i, P_{mi}, E_i are assumed to be constant throughout the transient period. Thereby, the P-δ curves provided by Equations (5) and (6) can be plotted as in Figure 4. P_{eO}, P_{eD}, P_{eP} are the pre-fault, during fault and post-fault values of P_e respectively. δ_O, δ_τ are the pre-fault value and the fault clearing moment value of δ respectively. N is the system's pre-fault operating point. A_{acc}, A_{decmax} are the equivalent accelerating area and the equivalent maximum decelerating area of the whole system respectively.

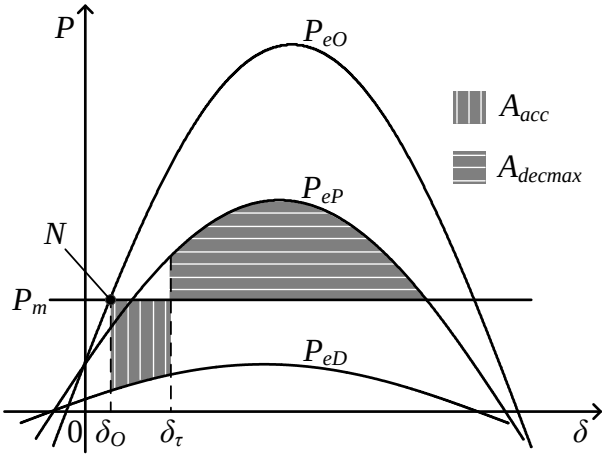

Figure 4. P-δ curves of the equivalent one-machine infinite-bus (OMIB) system.

The transient stability of a multi-machine power system can be assessed by using equal area criterion combined with the equivalent power curves plotted in Figure 4 [18]. An index to measure the system transient stability, which is called as the transient stability margin, is defined as:

$$V_{ts} = \frac{A_{decmax} - A_{acc}}{A_{acc}} = \frac{A_{decmax}}{A_{acc}} - 1 \tag{8}$$

The bigger the V_{ts}, the better the system transient stability. $V_{ts} > 0$ and $V_{ts} \leqslant 0$ correspond to the stable and unstable conditions, respectively. After integrating PMSGs into a multi-machine power system, the changes in the system's equivalent power curves mentioned above can reflect the impact of integrating PMSGs on the system transient stability. Therefore, based on the theory of EEAC, an analysis of these changes is carried out in the following section to study the influence mechanisms and find out some influence rules of integrating PMSGs on the transient stability of multi-machine power systems.

4. PMSG Impact Analysis

In this section, the transient stability of two cases are compared based on the theory of EEAC. One is the no-wind power case, which represents a multi-machine power system without PMSGs. The other one is the wind case, which is obtained by directly integrating PMSGs into the system of the no-wind power case. When the system loads keep unchanged, the newly added wind power is balanced by reducing the active power output of several original synchronous generators [9,27]. In these two cases, the fault conditions (fault type, fault location and fault duration) are the same in order to achieve a fair comparison.

In the wind case, four scenarios of system operation with different machines used to balance wind power and different PMSG's reactive power control modes are selected to study, as described in Table 1. All these four operating scenarios consider the most severe situation of integrating PMSGs. It is assumed that PMSG-based wind farms are all integrated into the cluster *S* when a grid fault occurs, which means that the mutual admittances between the integration nodes of wind farms and the generator nodes of the cluster *S* is great larger than that between the integration nodes of wind farms and the generator nodes of the cluster *A* [19].

Table 1. Four operating scenarios of the wind case.

Scenarios	Machines Used to Balance Wind Power	PMSG Control Mode
Scenario one	Remaining synchronous generators	Unity power factor
Scenario two	Remaining synchronous generators	Reactive power support
Scenario three	Critical synchronous generators	Unity power factor
Scenario four	Critical synchronous generators	Reactive power support

For example, in WSCC 3-machine-9-bus system [28], PMSG-based wind farms are integrated at bus 7 nearby generator G2, as shown in Figure 5. Generator G2 can belong to cluster *S* when a short-circuit fault occurs nearby bus 7. And generator G1, G3 can belong to cluster *A* in the same fault condition. When the wind power is balanced by reducing the active power output of generator G1 or G3, the operation of the system presented in Figure 5 will correspond to the scenario one or two. When the wind power is balanced by reducing the active power output of generator G2, the system operation will correspond to the scenario three or four. Naturally, the scenarios listed in Table 1 can also occur in other systems.

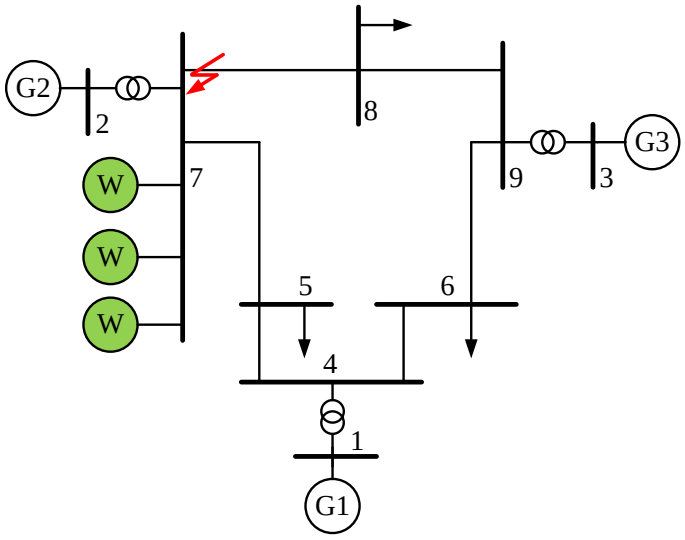

Figure 5. Western Systems Coordinating Council (WSCC) 3-machine-9-bus system integrated with PMSG-based wind farms.

4.1. Scenario One

As discussed in Section 2, a PMSG behaves as a controlled current source when it experiences grid faults, so a PMSG does not possess transient power-angle characteristics like a conventional synchronous generator or show any inertia to the grid. A PMSG has no problem of rotor angle stability itself and its generator does not synchronize with other conventional synchronous generators. As a result, after integrating PMSGs, the inertia of the whole system stays unchanged and the rotor motion equations of PMSGs will not be included in the expression derivation of the system's

equivalent power presented in Section 3, which is still only based on the rotor motion equations of the original synchronous generators. Therefore, Equations (5) and (6) are applicable too in the wind case.

In scenario one, the synchronous generators used to balance wind power belong to the cluster A. Their active power output is reduced through scaling down the mechanical input power. Other synchronous generators maintain the original operating states. Their mechanical input power is unchanged compared with the no-wind power case. The corresponding equations are described by:

$$\begin{cases} \sum\limits_{i \in S} P_{mi1} = \sum\limits_{i \in S} P_{mi0} \\ \sum\limits_{j \in A} P_{mj1} = \sum\limits_{j \in A} P_{mj0} - P_{ePMSG} \end{cases} \tag{9}$$

where, P_{mi1}, P_{mi0} are the mechanical input power of the i-th synchronous generator of the wind case operating in scenario one and of the no-wind power case respectively. P_{mj1}, P_{mj0} are the mechanical input power of the j-th synchronous generator of the wind case operating in scenario one and of the no-wind power case respectively. P_{ePMSG} is the pre-fault value of the sum of all the integrated PMSGs' active power outputs.

According to Equations (5) and (9), it can be known that the value of P_m of the wind case operating in scenario one, which is represented by P_{m1}, is bigger than that of the no-wind power case, as described by:

$$P_{m1} = P_{m0} + \frac{M_S}{M_S + M_A} P_{ePMSG} \tag{10}$$

where, P_{m0} is the value of P_m of the no-wind power case.

As stated in Section 3, the mechanical input power of every conventional synchronous generator is always assumed to be constant and keep its pre-fault value throughout the study period of transient stability. Therefore Equations (9) and (10) are valid throughout the same period. P_{m1} and P_{m0} are also constant like the P_m plotted in Figure 4. From Equation (10), it can be known that the incremental amount of P_{m1} compared with P_{m0} depends on the pre-fault value of the active power outputted by PMSGs. Considering the system's most stressed pre-fault operating point, it is assumed that all the PMSGs operate at their rated active power before grid faults happen [9], so P_{m1} can be determined by the wind power penetration level, which is the ratio between the rated values of the PMSGs' active power output and the total load [14]. The higher the wind power penetration level, the bigger the P_{m1}.

Because the output current of a PMSG is variable during the study period of transient stability, it is difficult to figure out the impact of integrating PMSGs on the system's equivalent electrical output power by directly comparing the wind case with the no-wind power case, so another case is added into the analysis as a reference case to solve this problem. This reference case is obtained by integrating ideal constant current sources (CCSs) into the system of the no-wind power case. It is thus denoted as the CCS case. At first, considering the same grid fault, the P_e curves of the wind case and the no-wind power case will be compared with those of the CCS case respectively, because these comparisons are easier to get results. Afterwards, the obtained comparison results will be analyzed together to find out the differences between the P_e curves of the wind and no-wind power cases.

In the CCS case, the output current of a CCS is equal to the pre-fault value of the PMSG's output current, as shown in Figure 6. A CCS also has the same rated active power output as a PMSG. The integration points of CCSs, the CCS power penetration level that is the ratio between the rated values of the CCSs' active power output and the total load, the machines used to balance the CCS power are all the same as those of the PMSGs in the wind case. Therefore, corresponding to the four operating scenarios of the wind case, the CCS case has two operating scenarios considered in the analysis, as shown in Table 2. The CCS case operating in the scenario I or II is denoted by the CCS case I and the CCS case II respectively.

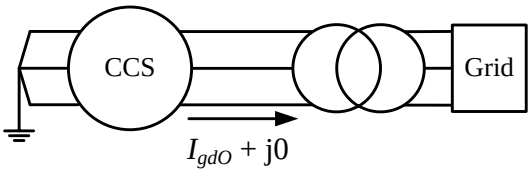

Figure 6. A constant current source (CCS) integrated into the grid.

Table 2. Two operating scenarios of the CCS case.

Scenarios	Machines Used to Balance the CCS Power	Corresponding Operating Scenarios of the Wind Case
Scenario I	Remaining synchronous generators	Scenario one, Scenario two
Scenario II	Critical synchronous generators	Scenario three, Scenario four

A CCS has no rotor or rotor motion equation. After integrating CCSs, the derivation of the system's equivalent electrical output power is still only based on the rotor motion equations of the original synchronous generators. Equation (6) is thus also applicable in the CCS case. In addition, the integration of CCSs does not influence the system's inertia and admittance matrix. According to Equations (6) and (7), it can be known that the P_e curves of the CCS case remain the same as the ones of the no-wind power case, no matter which scenario the CCS case is operating in. The corresponding equations are described by:

$$\begin{cases} P_{eO\mathrm{I}} = P_{eO\mathrm{II}} = P_{eO0} \\ P_{eD\mathrm{I}} = P_{eD\mathrm{II}} = P_{eD0} \\ P_{eP\mathrm{I}} = P_{eP\mathrm{II}} = P_{eP0} \end{cases} \tag{11}$$

where, $P_{eO\mathrm{I}}$, $P_{eD\mathrm{I}}$, $P_{eP\mathrm{I}}$ are the values of the P_{eO}, P_{eD} and P_{eP} curves of the CCS case I respectively. $P_{eO\mathrm{II}}$, $P_{eD\mathrm{II}}$, $P_{eP\mathrm{II}}$ are the values of the P_{eO}, P_{eD} and P_{eP} curves of the CCS case II respectively. P_{eO0}, P_{eD0}, P_{eP0} are the values of the P_{eO}, P_{eD} and P_{eP} curves of the no-wind power case respectively.

As analyzed in Section 2, a PMSG of the wind case behaves like a CCS of the CCS case during the pre-fault and the post-fault periods. Therefore, considering other same settings of the wind case and the CCS case, the values of the P_{eO} and P_{eP} curves of the wind case are equal to those of the CCS case. According to Equation (11), they are also equal to those of the no-wind power case. As a result, after integrating PMSGs, the system's P_{eO} and P_{eP} curves will keep their original forms. In scenario one, the corresponding equations are described by:

$$\begin{cases} P_{eO1} = P_{eO\mathrm{I}} = P_{eO0} \\ P_{eP1} = P_{eP\mathrm{I}} = P_{eP0} \end{cases} \tag{12}$$

where, P_{eO1}, P_{eP1} are the values of the P_{eO} and P_{eP} curves of the wind case operating in scenario one respectively.

If grid faults occur, the output current of a PMSG will change to a different value from its pre-fault value. In the wind case operating in scenario one, the fault period output current of a PMSG is an active current that is bigger than I_{gdO}, while the fault period output current of a CCS in the CCS case I is still equal to I_{gdO}, so in the wind case, the bigger active current injection from PMSGs makes the transmission lines near PMSGs possess larger current magnitudes compared with the same lines in the CCS case I. These transmission lines in the wind case thus have more active and reactive power losses, which can cause the network near PMSGs to have a lower voltage. Therefore, the critical synchronous generators near PMSGs may output less active power during the fault period, compared with the same critical machines in the CCS case I, but the remaining synchronous generators in the wind case can barely be influenced due to their long electrical distances from the PMSGs [14]. Their fault period active power generation may be equal to that of the remaining machines in the CCS case

I, with considering the same settings of the wind case and the CCS case previously introduced. The corresponding equations are described by:

$$\begin{cases} \sum\limits_{i\in S} P_{eDi1} < \sum\limits_{i\in S} P_{eDiI} \\ \sum\limits_{j\in A} P_{eDj1} = \sum\limits_{j\in A} P_{eDjI} \end{cases} \tag{13}$$

where, P_{eDi1}, P_{eDj1} are the during fault values of the electrical output power of the i-th and j-th synchronous generators in the wind case operating in scenario one respectively. P_{eDiI}, P_{eDjI} are the during fault values of the electrical output power of the i-th and j-th synchronous generators in the CCS case I respectively.

According to Equations (6) and (13), it can be known that the P_{eD} curve value of the wind case operating in scenario one is smaller than that of the CCS case I, as described by:

$$\begin{aligned} &\left(P_{eD1} = \frac{1}{M_S + M_A}\left(M_A \sum_{i\in S} P_{eDi1} - M_S \sum_{j\in A} P_{eDj1}\right)\right) \\ <&\left(P_{eDI} = \frac{1}{M_S + M_A}\left(M_A \sum_{i\in S} P_{eDiI} - M_S \sum_{j\in A} P_{eDjI}\right)\right) \end{aligned} \tag{14}$$

where, P_{eD1} is the value of the P_{eD} curve of the wind case operating in scenario one.

According to Equations (11) and (14), P_{eD1} is also smaller than P_{eD0}. Therefore, the system's P_{eD} curve can be brought down after integrating PMSGs with the unity power factor control mode, as described by:

$$P_{eD1} < P_{eDI} = P_{eD0} \tag{15}$$

Based on Equations (10), (12) and (15), the comparison of the equivalent P-δ curves between the wind and no-wind power cases is shown in Figure 7. N_0, δ_{O0}, $\delta_{\tau 0}$, A_{acc0}, $A_{decmax0}$ are the variables of the no-wind power case. They represent the system's pre-fault operating point, the pre-fault value of δ, the fault clearing moment value of δ, the equivalent accelerating area and the equivalent maximum decelerating area of the whole system, respectively. N_1, δ_{O1}, $\delta_{\tau 1}$, A_{acc1}, $A_{decmax1}$ are the corresponding variables of the wind case operating in scenario one.

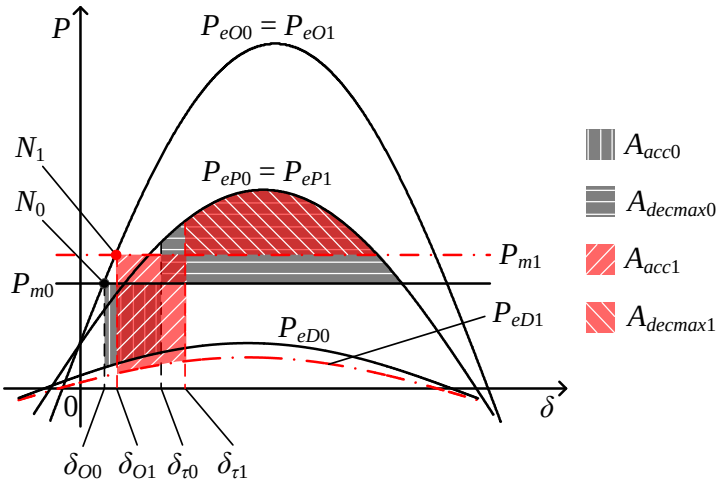

Figure 7. The comparison of the equivalent P-δ curves between the wind case operating in scenario one and the no-wind power case.

Observing Figure 7, it can be seen that the pre-fault operating point of the wind case is higher than that of the no-wind power case because of the P_{m1} curve rise, so $\delta_{O1} > \delta_{O0}$. The accelerating power of the wind case, $(P_{m1} - P_{eD1})$, is larger than that of the no-wind power case due to the P_{m1} curve rise and the P_{eD1} curve drop. Therefore, according to Equation (3), it can be deduced that the equivalent rotor angle variation of the wind case is larger too during the fault period, with considering the same fault duration in these two cases. The corresponding equation is shown below:

$$(\delta_{\tau 1} - \delta_{O1}) > (\delta_{\tau 0} - \delta_{O0}) \tag{16}$$

Considering $\delta_{O1} > \delta_{O0}$ and Equation (16), it can be known that $\delta_{\tau 1}$ is bigger than $\delta_{\tau 0}$. As a result, compared with the no-wind power case, it can be seen from Figure 7 that the equivalent accelerating area of the wind case is increased due to the P_{m1} curve rise, P_{eD1} curve drop and the increment of $\delta_{\tau 1} - \delta_{O1}$. The equivalent maximum decelerating area of the wind case is decreased due to the P_{m1} curve rise and the increment of $\delta_{\tau 1}$. The corresponding equation is shown below:

$$\begin{cases} A_{acc1} > A_{acc0} \\ A_{decmax1} < A_{decmax0} \end{cases} \tag{17}$$

According to Equations (8) and (17), Equation (18) can be obtained. The transient stability of the wind case is worse than that of the no-wind power case:

$$\left(V_{ts1} = \frac{A_{decmax1}}{A_{acc1}} - 1\right) < \left(V_{ts0} = \frac{A_{decmax0}}{A_{acc0}} - 1\right) \tag{18}$$

where, V_{ts0}, V_{ts1} are the transient stability indexes of the no-wind power case and the wind case operating in scenario one respectively.

Therefore, the PMSG-based wind power penetration has a detrimental impact on the system transient stability in this analyzed situation. When the wind power penetration level increases, the system transient stability will become worse due to the higher P_{m1} curve and the lower P_{eD1} curve.

4.2. Scenario Two

In scenario two, the analysis of the system's P_m, P_{eO} and P_{eP} curves are similar to the scenario one. The analysis results are shown below:

$$\begin{cases} P_{m2} = P_{m0} + \dfrac{M_S}{M_S + M_A} P_{ePMSG} \\ P_{eO2} = P_{eOI} = P_{eO0} \\ P_{eP2} = P_{ePI} = P_{eP0} \end{cases} \tag{19}$$

where, P_{m2}, P_{eO2}, P_{eP2} are the values of the P_m, P_{eO} and P_{eP} curves of the wind case operating in scenario two respectively.

If grid faults occur, a PMSG of the wind case operating in scenario two will output reactive current to improve the grid voltage, while a CCS of the CCS case I will still only output active current. So in the wind case, the network near PMSGs can possesses higher voltage compared with the same part of the grid in the CCS case I. As a result, the critical synchronous generators near PMSGs may output more active power during the fault period, compared with the same critical machines in the CCS case I. The remaining synchronous generators in the wind case still receive little impact from the fault period output current of PMSGs and have the same active power output as the remaining machines in the CCS case I. Therefore, according to Equations (6) and (11), the value of the P_{eD} curve

of the wind case operating in scenario two is larger than that of the CCS case I, and is thus larger than that of the no-wind power case. The corresponding equation is shown below:

$$P_{eD2} > P_{eDI} = P_{eD0} \tag{20}$$

where, P_{eD2} is the value of the P_{eD} curve of the wind case operating in scenario two.

Based on Equations (19) and (20), the comparison of the equivalent P-δ curves between the wind and no-wind power cases is shown in Figure 8. N_2, δ_{O2}, $\delta_{\tau 2}$, A_{acc2}, $A_{decmax2}$ are the variables of the wind case operating in scenario two. They represent the system's pre-fault operating point, the pre-fault value of δ, the fault clearing moment value of δ, the equivalent accelerating area and the equivalent maximum decelerating area of the whole system, respectively.

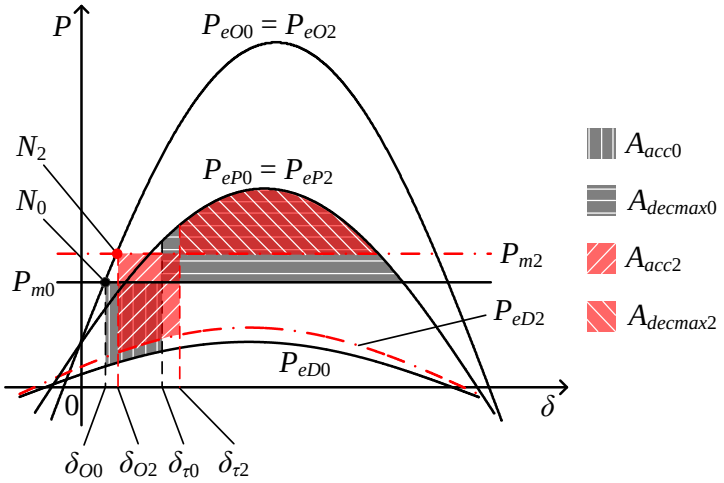

Figure 8. The comparison of the equivalent P-δ curves between the wind case operating in scenario two and the no-wind power case.

Observing Figure 8, compared with the no-wind power case, it can be seen that both the values of the P_{m2} and P_{eD2} curves are increased. However, the reactive power support capability of PMSGs is restricted by the capacity of converters and the grid voltage drop [10]. The voltage improvement of the network near PMSGs is limited and so is the rise of the P_{eD2} curve. The P_{m2} curve thus has a larger rise amount. As a result, the accelerating power of the wind case, $(P_{m2} - P_{eD2})$, is still larger than that of the no-wind power case. During the fault period, the equivalent rotor angle of the wind case also has larger variation, as described by:

$$(\delta_{\tau 2} - \delta_{O2}) > (\delta_{\tau 0} - \delta_{O0}) \tag{21}$$

Compared with the no-wind power case, the equivalent accelerating area of the wind case is increased due to the increment of $\delta_{\tau 2} - \delta_{O2}$ and the P_{m2} curve rise, which has greater effect than the P_{eD2} curve rise. The equivalent maximum decelerating area of the wind case is decreased due to the P_{m2} curve rise and the increment of $\delta_{\tau 2}$. Therefore, the transient stability of the wind case is still worse than that of the no-wind power case, as described by:

$$V_{ts2} < V_{ts0} \tag{22}$$

where, V_{ts2} is the transient stability index of the wind case operating in scenario two. In this analyzed situation, the PMSG-based wind power penetration also has a detrimental impact on the system transient stability. When the wind power penetration level increases, the system transient stability

will become worse too due to the higher P_{m2} curve, which has greater effect on the system than the higher P_{eD2} curve.

Observing Figures 7 and 8 together, the P_m curves and the pre-fault operating points of the wind cases operating in scenario one and two will be the same when the wind power penetration level is equal in these two scenarios, but the accelerating power of the wind case operating in scenario two is smaller due to the P_{eD2} curve rise compared with the P_{eD1} curve drop. Therefore, the equivalent rotor angle of the wind case operating in scenario two has smaller variation during the fault period, as described by:

$$(\delta_{\tau 2} - \delta_{O2}) < (\delta_{\tau 1} - \delta_{O1}) \tag{23}$$

Considering the same pre-fault operating points of the wind cases operating in these two scenarios and Equation (23), it can be known that $\delta_{\tau 2}$ is smaller than $\delta_{\tau 1}$, so compared with scenario one, the equivalent accelerating area of the wind case operating in scenario two is decreased due to the higher P_{eD2} curve and the smaller $\delta_{\tau 2} - \delta_{O2}$. The equivalent maximum decelerating area of the wind case operating in scenario two is increased due to the smaller $\delta_{\tau 2}$. Therefore, the wind case operating in scenario two has better transient stability.

4.3. Scenario Three

In scenario three, the synchronous generators used to balance wind power belong to the cluster *S*. Their active power output is also reduced through scaling down the mechanical input power. Other synchronous generators maintain the original operating states. The corresponding equations are described by:

$$\begin{cases} \sum\limits_{i \in S} P_{mi3} = \sum\limits_{i \in S} P_{mi0} - P_{ePMSG} \\ \sum\limits_{j \in A} P_{mj3} = \sum\limits_{j \in A} P_{mj0} \end{cases} \tag{24}$$

where, P_{mi3}, P_{mj3} are the mechanical input power of the *i*-th and *j*-th synchronous generators of the wind case operating in scenario three respectively.

According to Equations (5) and (24), it can be known that the value of P_m of the wind case operating in scenario three, which is represented by P_{m3}, is smaller than that of the no-wind power case, as described by:

$$P_{m3} = P_{m0} - \frac{M_A}{M_S + M_A} P_{ePMSG} \tag{25}$$

Like the analysis results in scenario one, Equations (24) and (25) are also valid throughout the study period of transient stability. P_{m3} is also constant and determined by the wind power penetration level. The higher the wind power penetration level, the smaller the P_{m3}.

The analysis of the P_e curves of the wind case operating in scenario three is similar to the scenario one, but the CCS case II is adopted as the reference case. The analysis results are shown below:

$$\begin{cases} P_{eO3} = P_{eOII} = P_{eO0} \\ P_{eD3} < P_{eDII} = P_{eD0} \\ P_{eP3} = P_{ePII} = P_{eP0} \end{cases} \tag{26}$$

where, P_{eO3}, P_{eD3}, P_{eP3} are the values of the P_{eO}, P_{eD} and P_{eP} curves of the wind case operating in scenario three respectively.

Based on Equations (25) and (26), the comparison of the equivalent *P*-δ curves between the wind and no-wind power cases is shown in Figure 9. N_3, δ_{O3}, $\delta_{\tau 3}$, A_{acc3}, $A_{decmax3}$ are the variables of the wind case operating in scenario three. They represent the system's pre-fault operating point, the pre-fault value of δ, the fault clearing moment value of δ, the equivalent accelerating area and the equivalent maximum decelerating area of the whole system, respectively.

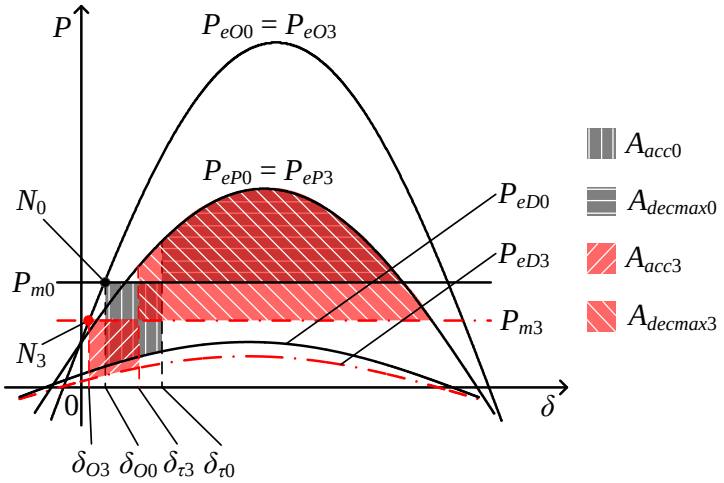

Figure 9. The comparison of the equivalent *P*-δ curves between the wind case operating in scenario three and the no-wind power case.

Observing Figure 9, it can be seen that the pre-fault operating point of the wind case is lower than that of the no-wind power case because of the P_{m3} curve drop. So $\delta_{O3} < \delta_{O0}$. The value of the P_{eD3} curve is also decreased compared with the P_{eD0} curve. During the fault period, the output current increment of PMSGs with the unity power factor control mode is the main reason to cause the P_{eD3} curve drop. But this current increment is limited especially in the high wind speed situation. So the drop of the P_{eD3} curve may be not significant and the P_{m3} curve has larger drop amount. As a result, the accelerating power of the wind case, $(P_{m3} - P_{eD3})$, is smaller than that of the no-wind power case. The equivalent rotor angle of the wind case thus has smaller fault period variation, as described by:

$$(\delta_{\tau 3} - \delta_{O3}) < (\delta_{\tau 0} - \delta_{O0}) \tag{27}$$

Considering $\delta_{O3} < \delta_{O0}$ and Equation (27), it can be known that $\delta_{\tau 3}$ is smaller than $\delta_{\tau 0}$. Compared with the no-wind power case, the equivalent accelerating area of the wind case is decreased due to the decrement of $\delta_{\tau 3} - \delta_{O3}$ and the P_{m3} curve drop, which has greater effect than the P_{eD3} curve drop. The equivalent maximum decelerating area of the wind case is increased due to the P_{m3} curve drop and the decrement of $\delta_{\tau 3}$. Therefore, the transient stability of the wind case is better than that of the no-wind power case, as described by:

$$V_{ts3} > V_{ts0} \tag{28}$$

where, V_{ts3} is the transient stability index of the wind case operating in scenario three. In this analyzed situation, the PMSG-based wind power penetration has a beneficial impact on the system transient stability. When the wind power penetration level increases, the system transient stability will become better due to the lower P_{m3} curve, which has greater effect on the system than the lower P_{eD3} curve.

4.4. Scenario Four

In scenario four, the analysis of the system's P_m curve is similar to the scenario three and the analysis of the system's P_e curves is similar to the scenario two. The CCS case II is used as the reference case. The analysis results of scenario four are shown below:

$$\begin{cases} P_{m4} = P_{m0} - \dfrac{M_A}{M_S + M_A} P_{ePMSG} \\ P_{eO4} = P_{eOII} = P_{eO0} \\ P_{eD4} > P_{eDII} = P_{eD0} \\ P_{eP4} = P_{ePII} = P_{eP0} \end{cases} \tag{29}$$

where, P_{m4}, P_{eO4}, P_{eD4}, P_{eP4} are the values of the P_m, P_{eO}, P_{eD} and P_{eP} curves of the wind case operating in scenario four respectively. P_{m4} is constant throughout the study period of transient stability.

Based on Equation (29), the comparison of the equivalent P-δ curves between the wind and no-wind power cases is shown in Figure 10. N_4, δ_{O4}, $\delta_{\tau 4}$, A_{acc4}, $A_{decmax4}$ are the variables of the wind case operating in scenario four. They represent the system's pre-fault operating point, the pre-fault value of δ, the fault clearing moment value of δ, the equivalent accelerating area and the equivalent maximum decelerating area of the whole system, respectively.

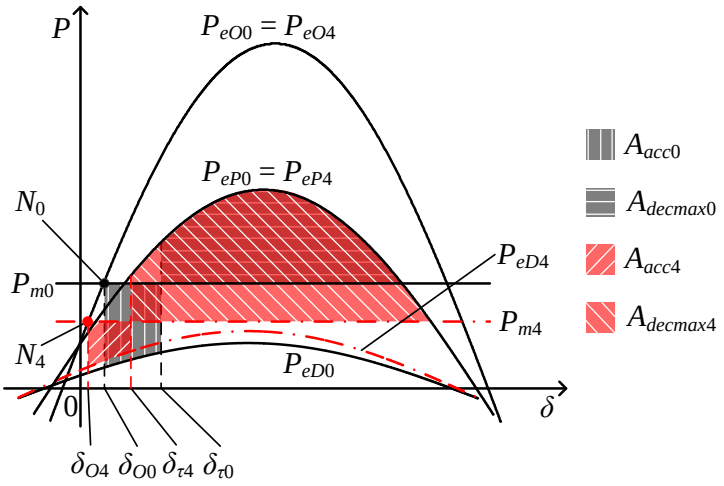

Figure 10. The comparison of the equivalent P-δ curves between the wind case operating in scenario four and the no-wind power case.

Observing Figure 10, it can be seen that the pre-fault operating point of the wind case is also lower than that of the no-wind power case because of the P_{m4} curve drop. The accelerating power of the wind case, $(P_{m4} - P_{eD4})$, is smaller than that of the no-wind power case due to the P_{m4} curve drop and the P_{eD4} curve rise. As a result, during the fault period, the equivalent rotor angle of the wind case has smaller variation, as described by:

$$(\delta_{\tau 4} - \delta_{O4}) < (\delta_{\tau 0} - \delta_{O0}) \tag{30}$$

Compared with the no-wind power case, it can be seen from Figure 10 that the equivalent accelerating area of the wind case is decreased due to the P_{m4} curve drop, P_{eD4} curve rise and the decrement of $\delta_{\tau 4} - \delta_{O4}$. The equivalent maximum decelerating area of the wind case is increased due to the P_{m4} curve drop and the decrement of $\delta_{\tau 4}$. Therefore, the transient stability of the wind case is still better than that of the no-wind power case, as described by:

$$V_{ts4} > V_{ts0} \tag{31}$$

where, V_{ts4} is the transient stability index of the wind case operating in scenario four. In this analyzed situation, the PMSG-based wind power penetration also has a beneficial impact on the system transient stability. When the wind power penetration level increases, the system transient stability will become better due to the lower P_{m4} curve and the higher P_{eD4} curve.

Observing Figures 9 and 10 together, the P_m curves and the pre-fault operating points of the wind cases operating in scenario three and four will be the same when the wind power penetration level is equal in these two scenarios. The accelerating power of the wind case operating in scenario four is

smaller due to the P_{eD4} curve rise compared with the P_{eD3} curve drop. Therefore, the equivalent rotor angle of the wind case operating in scenario four has smaller fault period variation, as described by:

$$(\delta_{\tau 4} - \delta_{O4}) < (\delta_{\tau 3} - \delta_{O3}) \tag{32}$$

Consequently, $\delta_{\tau 4}$ is smaller than $\delta_{\tau 3}$. Compared with scenario three, the equivalent accelerating area of the wind case operating in scenario four is decreased due to the higher P_{eD4} curve and the smaller $\delta_{\tau 4} - \delta_{O4}$. The equivalent maximum decelerating area of the wind case operating in scenario four is increased due to the smaller $\delta_{\tau 4}$. Therefore, the wind case operating in scenario four has better transient stability.

4.5. Summary

Based on the above analysis, it can be concluded that the integration of PMSGs can change the system's equivalent mechanical input power and fault period electrical output power curves, when the newly added wind power is balanced by reducing the active power output of some original synchronous generators. The system's pre-fault operating point, equivalent accelerating and maximum decelerating areas are also affected, except for the system inertia.

The variations of the system's equivalent power curves caused by integrating PMSGs, such as the rise of the P_m curve and the drop of the P_{eD} curve can make A_{acc} increase and A_{decmax} decrease, which are harmful to the system transient stability. But the drop of the P_m curve and the rise of the P_{eD} curve can make A_{acc} decrease and A_{decmax} increase, which are good for the system transient stability. The integration of PMSGs may have either detrimental or beneficial impacts on the system transient stability.

The comparison results of the system transient stability obtained in the above analysis are summarized as follows:

$$V_{ts1} < V_{ts2} < V_{ts0} < V_{ts3} < V_{ts4} \tag{33}$$

In the situation of PMSGs integrated nearby the critical synchronous generators, the system transient stability will be degraded when the wind power is balanced by the remaining synchronous generators and will be improved when the wind power is balanced by the critical synchronous generators. In the same system, PMSGs using the reactive power support control mode can achieve better system transient stability compared with the usage of the unity power factor control mode. In addition, the increment of the wind power penetration level makes the impact of PMSGs become stronger.

5. Simulation Verification

In this section, dynamic simulations based on DIgSILENT/Power Factory are carried out as follows to verify the analysis results obtained in Section 4.

5.1. WSCC 3-Machine-9-Bus System

Firstly, the WSCC 3-machine-9-bus system presented in Figure 5 is adopted as a test system in our simulations. The three synchronous generators in the system are modeled as salient pole generators with AC excitation systems (IEEEX1). The load is modeled to include 33% constant current, 33% constant impedance, and 33% constant power [9]. A three-phase-to-ground fault with a certain fault impedance is applied on line 7–8 nearby bus 7. The fault occurs at 1 s and will be cleared by isolating the fault line.

In the original situation without wind power penetration, the critical clearing time (CCT) of the fault on line 7–8 is 130 ms. When the fault clearing time extends to 131 ms, the rotor angles of all the synchronous generators are measured with respect to the reference machine G1, as shown in Figure 11. It can be seen that the rotor angle of G2 spreads out fastest and loses the synchronism with

the rotor angles of other machines in the first swing. Therefore, G2 is the critical machine in this fault situation and belongs to the cluster *S*. G1 and G3 belong to the cluster *A*.

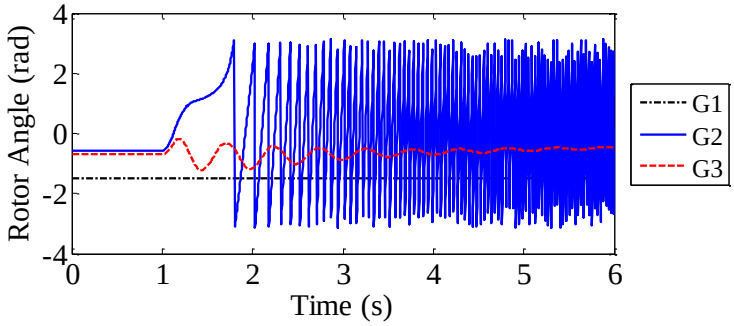

Figure 11. Rotor angles of synchronous generators with the 131 ms fault on line 7–8.

In the situation with wind power penetration, the same fault on line 7–8 is considered. To establish the operating scenarios studied in Section 4, PMSG-based wind farms are integrated at bus 7 near the critical synchronous generator G2. PMSGs in a wind farm are assumed to operate at their rated power with a constant wind speed of 12 m/s [9]. One wind farm is represented by an equivalent PMSG that is scaled to the size of the wind farm, which is 30 MW [29]. An equivalent PMSG is simulated by a controlled current source, as presented in Section 2.

At first, the wind power is balanced through reducing the active power output of a remaining synchronous generator G1. When the integrated PMSGs adopt the unity power factor control mode, the system operation corresponds to the scenario one analyzed in Section 4. When PMSGs adopt the reactive power support control mode, which follows the SDLWindV grid code, the system operation corresponds to the scenario two. In simulations, the wind power penetration level is increased by integrating more wind farms. The largest wind power penetration level of 30% is obtained by integrating three wind farms at bus 7. In these simulation scenarios, the CCTs of the fault on line 7–8 are recorded in Figure 12. CCT_0 represents the fault CCT in the original situation without wind power penetration.

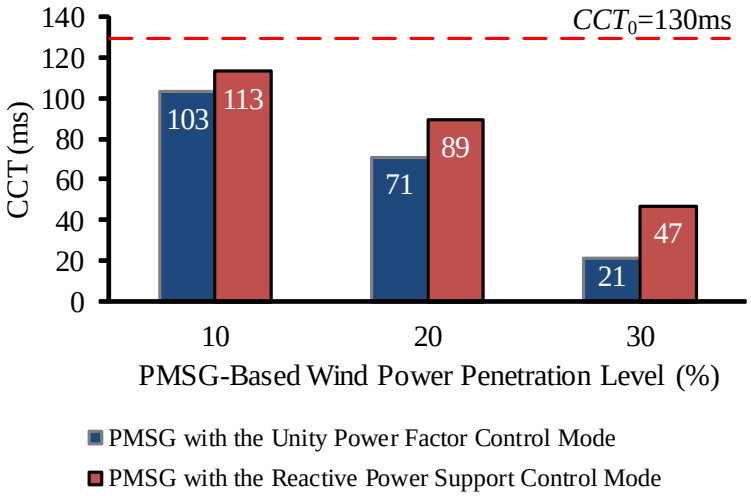

Figure 12. Critical clearing times (CCTs) of the fault on line 7–8 in the scenarios of PMSG-based wind power balanced by G1.

From Figure 12, it can be seen that all the CCTs are smaller than 130 ms, which means that the transient stability of the test system is degraded by integrating PMSGs. When the wind power penetration level increases, the system transient stability becomes worse. Compared with the unity

power factor control mode, PMSGs using the reactive power support control mode can make the test system have better transient stability. These simulation results are all consistent with the influence rules of integrating PMSGs, which are obtained in Section 4.

Afterwards, the wind power is balanced through reducing the active power output of the critical synchronous generator G2. When PMSGs adopt the unity power factor control mode, the system operation corresponds to the scenario three. When PMSGs adopt the reactive power support control mode, the system operation corresponds to the scenario four. In these simulation scenarios, the fault CCTs are recorded in Figure 13.

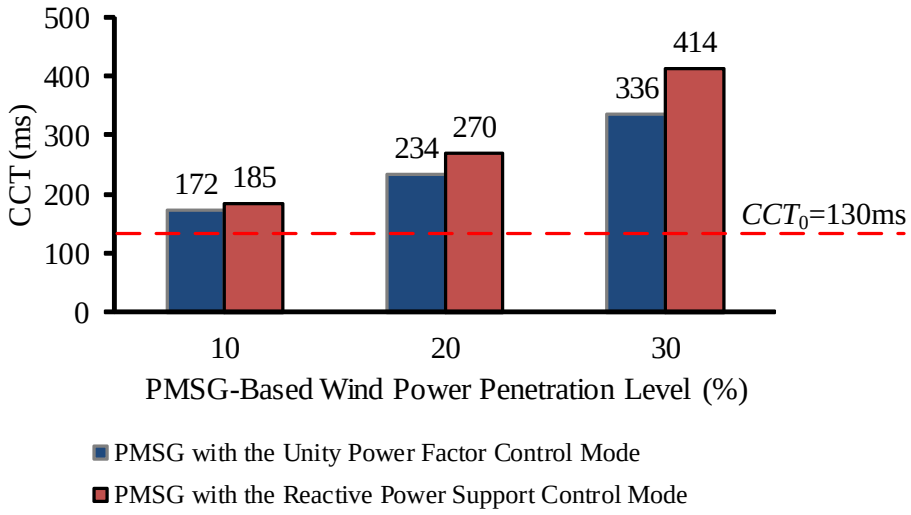

Figure 13. CCTs of the fault on line 7–8 in the scenarios of PMSG-based wind power balanced by G2.

From Figure 13, it can be seen that the system transient stability is improved by integrating PMSGs and becomes better when the wind power penetration level increases. The reactive power support control mode of PMSGs can contribute to the system transient stability. The simulation results shown in Figure 13 also have the same rules as Section 4 presented.

Observing Figures 12 and 13 together, it can be seen that the fault CCTs have a greater variation when the wind power is balanced by G2. For example, when the wind power penetration level is 30% and PMSGs use the unity power factor control mode, the percentage change of the fault CCT in Figure 13 is +158% ((336 ms − 130 ms)/130 ms) compared with the original fault CCT of 130 ms, while that in Figure 12 is only −84% ((21 ms − 130 ms)/130 ms). The reason of this phenomenon is that the cluster *S* only has G2 when the fault on line 7–8 is considered, so the equivalent inertia coefficient of the cluster *S* is smaller than that of the cluster *A*. According to Equations (10) and (25), the PMSG-based wind power balanced by G2 thus has larger impact on the system transient stability than the same amount of wind power balanced by G1. In addition, in these two figures, the differences of the fault CCTs caused by different PMSG control modes become more obvious when the wind power penetration level increases.

5.2. IEEE 10-Mahicne-39-Bus System

The analysis in Section 4 is further verified by using IEEE 10-machine-39-bus system [28], as shown in Figure 14. The round rotor generators with AC excitation systems (IEEET1) are used to simulate the ten synchronous generators in the system. The system load consists of constant current load, constant impedance load, and constant power load. The percentage of each type of load is 33%.

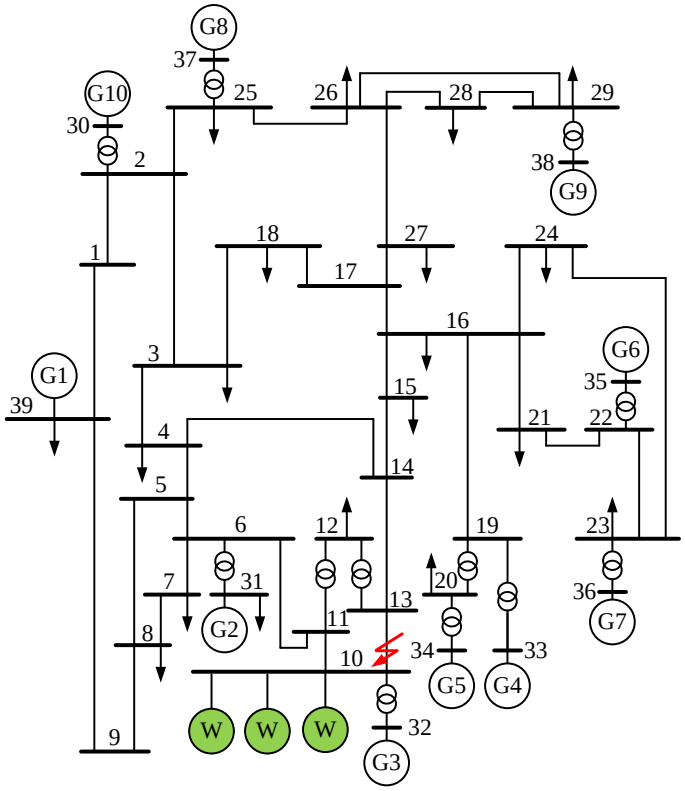

Figure 14. Institute of Electrical and Electronics Engineers (IEEE) 10-mahicne-39-bus system integrated with PMSG-based wind farms.

A three-phase-to-ground fault with a certain fault impedance is applied on line 10–13 nearby bus 10. Without wind power penetration, the CCT of this fault is 235 ms. When the fault clearing time extends to 236 ms, the rotor angles of all the synchronous generators are presented in Figure 15. It can be seen that G3 is the critical machine.

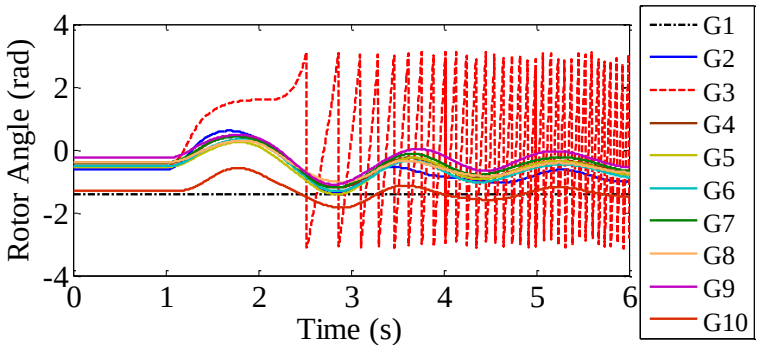

Figure 15. Rotor angles of synchronous generators with the 236 ms fault on line 10–13.

In the situation with wind power penetration, the same fault on line 10–13 is considered. PMSG-based wind farms are integrated at bus 10 nearby the critical synchronous generator G3. The rated active power output of one wind farm is 200 MW. At first, the wind power is balanced through reducing the active power output of a remaining synchronous generator G1. When PMSGs adopt the unity power factor control mode, the system operation corresponds to the scenario one. When PMSGs adopt the reactive power support control mode, which follows the SDLWindV grid code, the system operation corresponds to the scenario two. The largest wind power penetration

level of 10% is obtained by integrating three wind farms at bus 10, as shown in Figure 14. In these simulation scenarios, the CCTs of the fault on line 10–13 are recorded in Figure 16.

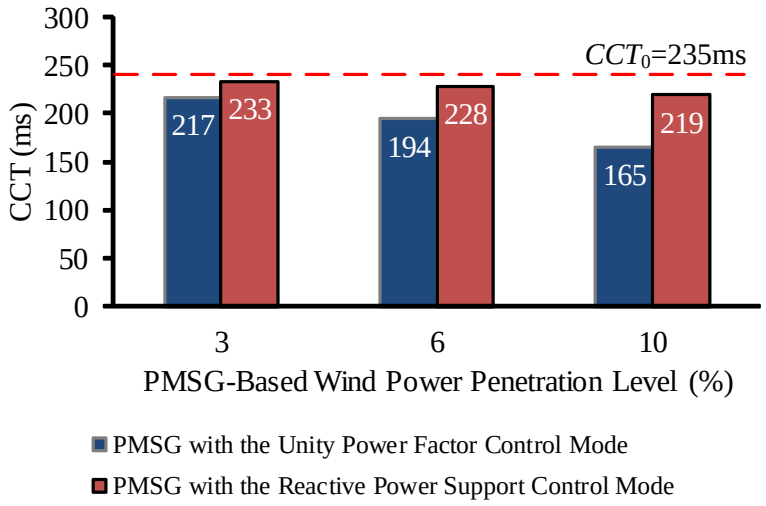

Figure 16. CCTs of the fault on line 10–13 in the scenarios of PMSG-based wind power balanced by G1.

From Figure 16, it can be seen that the system transient stability is degraded by integrating PMSGs and becomes worse when the wind power penetration level increases. Compared with the unity power factor control mode, PMSGs using the reactive power support control mode makes the test system have better transient stability. These simulation results are also consistent with the influence rules of integrating PMSGs obtained in Section 4.

Secondly, the wind power is balanced through reducing the active power output of the critical synchronous generator G3. When PMSGs use the unity power factor control mode, the system operation corresponds to the scenario three. When PMSGs use the reactive power support control mode, the system operation corresponds to the scenario four. The fault CCTs in these simulation scenarios are shown in Figure 17.

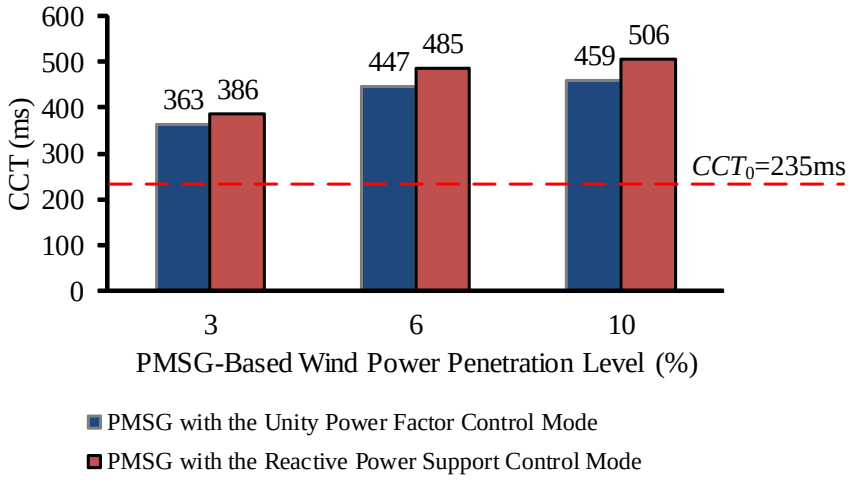

Figure 17. CCTs of the fault on line 10–13 in the scenarios of PMSG-based wind power balanced by G3.

From Figure 17, it can be seen that the transient stability of the test system is improved after integrating PMSGs and becomes better when the wind power penetration level increases. The largest CCT of the fault can be increased to 506 ms. The reactive power support control mode of PMSGs

can contribute to the system transient stability more than the unity power factor control mode. The simulation results shown in Figure 17 have the same rules as Section 4 presented.

The above simulation results of two test systems demonstrate that the influence rules of integrating PMSGs on the power system transient stability, which are obtained from the analysis in Section 4, are correct and applicable in different systems. The effectiveness of the analysis based on the EEAC theory is verified.

6. Conclusions

This paper analyzed the impact of integrating PMSGs on the transient stability of multi-machine power systems based on the theory of EEAC. According to the analysis results, it can be known that the integration of PMSGs influences the system transient stability through changing the system's equivalent power-angle relationships. The system's equivalent mechanical input power and the fault period electrical output power curves are mainly affected when the newly added PMSG-based wind power is balanced by reducing the active power output of original synchronous generators.

The selection of the machines used to balance wind power influences the system's equivalent mechanical input power, and it is the key factor to determine the impact of PMSGs. In the situation where PMSGs are integrated nearby the critical machines, the system transient stability will be degraded when wind power is balanced by the remaining machines, but it will be improved when wind power is balanced by critical machines. The reactive power control mode of PMSGs influences the system's equivalent fault period electrical output power. It may not be the decisive factor in determining whether the impact of PMSGs is detrimental or beneficial, due to the limitations of PMSGs' converter capacity. However, compared with the unity power factor control mode, PMSGs should adopt the reactive power support control mode that can achieve better system transient stability. In addition, the higher the wind power penetration level, the stronger the impact of integrating PMSGs.

Acknowledgments: This research work was supported by the Major Program of the National Natural Science Foundation of China (51190103), "111" Project (B08013) and China Scholarship Council. The authors are grateful for these supports.

Author Contributions: Zhongyi Liu is the main writer of the manuscript. Yong Liu discussed the research results and commented on the manuscript. Final review was done by Chongru Liu, Gengyin Li, and Yilu Liu. All the authors read and approved the final manuscript.

Conflicts of Interest: The authors declare no conflict of interest.

References

1. Global Wind Energy Council. *Global Wind Report Annual Market Update 2014*; Global Wind Energy Council: Brussels, Belgium, 2015; pp. 6–8.
2. Chen, J.; Chen, J.; Gong, C. On optimizing the aerodynamic load acting on the turbine shaft of PMSG-based direct-drive wind energy conversion system. *IEEE Trans. Ind. Electron.* **2014**, *61*, 4022–4031. [CrossRef]
3. Alepuz, S.; Calle, A.; Busquets-Monge, S.; Kouro, S.; Wu, B. Use of stored energy in PMSG rotor inertia for low-voltage ride-through in back-to-back NPC converter-based wind power systems. *IEEE Trans. Ind. Electron.* **2013**, *60*, 1787–1796. [CrossRef]
4. Dicorato, M.; Forte, G.; Trovato, M. Wind farm stability analysis in the presence of variable-speed generators. *Energy* **2012**, *39*, 40–47. [CrossRef]
5. Revel, G.; Leon, A.E.; Alonso, D.M.; Moiola, J.L. Dynamics and stability analysis of a power system with a PMSG-based wind farm performing ancillary services. *IEEE Trans. Circuits Syst.* **2014**, *61*, 2182–2193. [CrossRef]
6. Hossain, M.J.; Pota, H.R.; Mahmud, M.A.; Ramos, R.A. Investigation of the impacts of large-scale wind power penetration on the angle and voltage stability of power systems. *IEEE Syst. J.* **2012**, *6*, 76–84. [CrossRef]
7. Wu, F.; Zhang, X.P.; Ju, P. Small signal stability analysis and control of the wind turbine with the direct-drive permanent magnet generator integrated to the grid. *Electr. Power Syst. Res.* **2009**, *79*, 1661–1667. [CrossRef]

8. Sun, S.M.; Shi, L.B.; Ni, Y.X.; Yao, L.Z.; Bazargan, M. Impacts of Wind Power Intermittency on Power System Transient Stability. In Proceedings of the 9th IET International Conference on Advances in Power System Control, Operation and Management (APSCOM 2012), Hong Kong, China, 18–21 November 2012; pp. 1–5.
9. Vittal, E.; O'Malley, M.; Keane, A. Rotor angle stability with high penetrations of wind generation. *IEEE Trans. Power Syst.* **2012**, *27*, 353–362. [CrossRef]
10. Ullah, N.R.; Thiringer, T.; Karlsson, D. Voltage and transient stability support by wind farms complying with the E.ON Netz grid code. *IEEE Trans. Power Syst.* **2007**, *22*, 1647–1656. [CrossRef]
11. Mokui, H.T.; Masoum, M.A.; Mohseni, M.; Moghbel, M. Power System Transient Stability Enhancement Using Direct Drive Wind Generators. In Proceedings of the 2012 IEEE Power and Energy Society General Meeting, San Diego, CA, USA, 22–26 July 2012; pp. 1–6.
12. Rijcke, S.D.; Ergun, H.; Hertem, D.V.; Driesen, J. Grid impact of voltage control and reactive power support by wind turbines equipped with direct-drive synchronous machines. *IEEE Trans. Sustain. Energy* **2012**, *3*, 890–898. [CrossRef]
13. Ullah, N.R.; Thiringer, T. Variable speed wind turbines for power system stability enhancement. *IEEE Trans. Energy Convers.* **2007**, *22*, 52–60. [CrossRef]
14. Ullah, N.R.; Thiringer, T. Effect of operational modes of a wind farm on the transient stability of nearby generators and on power oscillations: A nordic grid study. *Wind Energy* **2008**, *11*, 63–73. [CrossRef]
15. Xu, Y.; Dong, Z.; Zhang, R.; Xue, Y.; Hill, D.J. A decomposition-based practical approach to transient stability-constrained unit commitment. *IEEE Trans. Power Syst.* **2015**, *30*, 1455–1464. [CrossRef]
16. El-Shimy, M. Stability-based minimization of load shedding in weakly interconnected systems for real-time applications. *Int. J. Electr. Power* **2015**, *70*, 99–107. [CrossRef]
17. Guo, H.; Xie, H.; Zhang, B.; Yu, G.; Li, P.; Bo, Z.; Klimek, A. Study on power system transient instability detection based on wide area measurement system. *Eur. Trans. Electr. Power* **2010**, *20*, 184–205. [CrossRef]
18. Xue, Y.; Cutsem, T.V.; Pavella, M.R. A simple direct method for fast transient stability assessment of large power systems. *IEEE Trans. Power Syst.* **1988**, *3*, 400–412. [CrossRef]
19. Lin, L.; Zhao, H.; Lan, T.; Wang, Q.; Zeng, J. Transient Stability Mechanism of DFIG Wind Farm and Grid-Connected Power System. In Proceedings of the 2013 IEEE Grenoble PowerTech, Grenoble, France, 16–20 June 2013; pp. 1–9.
20. Hansen, A.D.; Michalke, G. Multi-pole permanent magnet synchronous generator wind turbines' grid support capability in uninterrupted operation during grid faults. *IET Renew. Power Gener.* **2009**, *3*, 333–348. [CrossRef]
21. Gautam, D.; Vittal, V.; Harbour, T. Impact of increased penetration of DFIG-based wind turbine generators on transient and small signal stability of power systems. *IEEE Trans. Power Syst.* **2009**, *24*, 1426–1434. [CrossRef]
22. Ottersten, R.; Petersson, A.; Pietilainen, K. Voltage Sag Response of PWM Rectifiers for Variable-Speed Wind Turbines. In Proceedings of the 4th Nordic Workshop on Power and Industrial Electronics (NORpie 2004), Trondheim, Norway, 14–16 June 2004; pp. 1–8.
23. Asmine, M.; Brochu, J.; Fortmann, J. Model validation for wind turbine generator models. *IEEE Trans. Power Syst.* **2011**, *26*, 1769–1782. [CrossRef]
24. Federal Ministry for the Environment, Nature Conservation, Building and Nuclear Safety. *Ordinance on System Services by Wind Energy Plants (System Service Ordinance-SDLWindV)*; Federal Ministry for the Environment, Nature Conservation, Building and Nuclear Safety: Berlin, Germany, 2009.
25. Ellis, A.; Kazachkov, Y.; Muljadi, E.; Pourbeik, P.; Sanchez-Gasca, J.J. Description and Technical Specifications for Generic WTG Models—A Status Report. In Proceedings of the 2011 IEEE PES Power Systems Conference and Exposition, Phoenix, AZ, USA, 20–23 March 2011; pp. 1–8.
26. Kanellos, F.D.; Kabouris, J. Wind farms modeling for short-circuit level calculations in large power systems. *IEEE Trans. Power Del.* **2009**, *24*, 1687–1695. [CrossRef]
27. Yan, G.; Li, Y.; Mu, G.; Yuan, T.; Liu, H. Net Benefit Evaluation of Wind Power Considering Operational Regulation Cost of Thermal Plants for Balancing Wind Power. In Proceedings of the 2010 International Conference on Power System Technology, Hangzhou, China, 24–28 October 2010; pp. 1–7.

28. Nguyen, T.B.; Pai, M.A. Dynamic security-constrained rescheduling of power systems using trajectory sensitivities. *IEEE Trans. Power Syst.* **2003**, *18*, 848–854. [CrossRef]
29. Wang, L.; Thi, M.S. Stability enhancement of a PMSG-based offshore wind farm fed to a multi-machine system through an LCC-HVDC link. *IEEE Trans. Power Syst.* **2013**, *28*, 3327–3334. [CrossRef]